

Enhanced Uptake of [^{11}C]TPMP in Canine Brain Tumor: A PET Study

Igal Madar, James H. Anderson, Zsolt Szabo, Ursula Scheffel, Pan-Fu Kao, Hayden T. Ravert and Robert F. Dannals

Department of Radiology, Division of Nuclear Medicine, Johns Hopkins University School of Medicine, Baltimore, Maryland

In vitro studies have demonstrated the membrane potential-dependent enhanced uptake of phosphonium salts, including [^3H]triphenylmethylphosphonium (TPMP), into mitochondria of carcinoma and glioma-derived tumor cells, suggesting the potential use of phosphonium salts as tracers for tumor imaging. This study characterizes the in vivo uptake of [^{11}C]TPMP in canine brain glioma using PET. **Methods:** Dynamic paired PET studies of [^{11}C]TPMP followed by [^{68}Ga]ethylenediaminetetraacetic acid (EDTA) were performed 4 d before and 9 d after tumor cell inoculation. Graphical analysis was used to evaluate [^{11}C]TPMP retention in tumor tissue. Distribution of tracer uptake was compared with tumor histological sections. **Results:** [^{11}C]TPMP exhibited enhanced uptake and prolonged retention in tumor cells. Patlak plot was linear over the 20- to 95-min postinjection period ($r = 0.97 \pm 0.1$). [^{68}Ga]EDTA exhibited a gradual washout from the tumor tissue. The tumor-to-normal brain uptake ratio at 55 to 95 min postinjection was 47.5 for [^{11}C]TPMP and 8.1 for [^{68}Ga]EDTA. Qualitative comparison with histological sections indicated that [^{11}C]TPMP enhanced uptake was restricted to the tumor area. **Conclusion:** The enhanced uptake and prolonged retention in tumor suggest [^{11}C]TPMP as a promising means for imaging of gliomas in dogs. The need for studies in humans is indicated.

Key Words: [^{11}C]triphenylmethylphosphonium; glioma; dog; PET
J Nucl Med 1999; 40:1180–1185

Despite recent technological advances and development of new tracers, diagnostic imaging of brain tumors continues to be a challenging problem. Contrast-enhanced CT and MRI can provide detailed anatomic delineation of a malignant lesion, but they are of low diagnostic value for the differentiation between low-grade and high-grade tumors and between recurrent or residual tumors and necrotic tissue (1). Also, they cannot detect early physiological and biochemical changes in response to treatment, which may occur before anatomic alterations (2). PET and SPECT imaging of radionuclides, targeting specific biochemical and physiological abnormalities characteristic of neoplastic cells, may complement some of the shortcomings of radiographic imaging.

Received Jul. 22, 1998; revision accepted Nov. 5, 1998.
For correspondence or reprints contact: Igal Madar, PhD, Division of Nuclear Medicine, Johns Hopkins University School of Medicine, 601 N. Carolina St./JHDC 4230, Baltimore, MD 21282-0855.

A number of PET and SPECT tracers, which detect malignant lesions caused by enhanced metabolic activities or interruptions in membrane transport mechanisms, have been developed (3–13). However, the tumor uptake of most of these radioligands provides rather low tumor-to-normal brain uptake ratios that may range between 0.5 and 3.0. Low tumor-to-background contrast may impair the visual resolution of malignant lesions in cases such as occult tumors, low-grade neoplasms, rim-shaped high-grade tumors and small malignant lesions.

In this study, we investigated the uptake of the radiolabeled lipophilic cation [^{11}C]triphenylmethylphosphonium (TPMP) in canine brain gliomas. Numerous in vitro studies have demonstrated the unusual accumulation of [^3H]tetraphenylphosphonium (TPP) and [^3H]TPMP in the plasma and mitochondria of a wide variety of cell lines (14–20). Accumulation of these ions in the human breast carcinoma MCF-7 cell line was >30 times higher than in normal epithelial cells (14). A similar uptake ratio was found in dispersed cells taken from human brain glioma (15). Tumor selectivity of radiolabeled phosphonium ions has also been validated in in vivo models. [^3H]TPP accumulation in glioma cells inoculated in the rat's brain was 20 times higher than in the intact contralateral brain (21,22). We have found [^3H]TPP activity in lung nodules induced by intravenous injection of Lewis lung carcinoma cells to be six times higher than in normal lung parenchyma (23). This study analyzes the kinetics of [^{11}C]TPMP in canine brain glioma under in vivo conditions directly applicable to human studies, to assess its suitability as a PET tracer for tumor detection.

MATERIALS AND METHODS

The animal studies were approved by the Johns Hopkins Animal Care and Use Committee. Gliosarcoma cells derived from Rouse avian sarcoma virus, grown subcutaneously in nude mice, were used in this study (24). The mice were killed, and tumor nodules (3–7 mm in diameter) were removed, mechanically dissociated and suspended in a solution of RPMI 1640 medium (GIBCO, Bethesda, MD) to a final concentration of 1.2×10^7 viable cells/mL. Tumors were induced in three adult purebred beagle dogs (8–10 kg), as previously described (25). The dogs were anesthetized with intravenous sodium pentobarbital (35 mg/kg), and sterile surgical techniques were used to expose the midline surface of the skull. A 1-mm-diameter cranial burr hole was created (1 cm lateral to the sagittal suture, 0.5 cm distal to the coronal suture). Thirty

microliters tumor suspension were injected into the parenchyma through a 23-gauge needle attached to a 100- μ L syringe to a depth of 1 cm. The muscles and skin were closed, the location of the burr hole was marked on the skin using a suture and the dogs were monitored during recovery from anesthesia.

Synthesis of [^{11}C]TPMP Iodide

[^{11}C]TPMP was prepared by methylation of triphenylphosphonium with [^{11}C]methyl iodide as previously described (26). Briefly, $^{11}\text{CH}_3\text{I}$ was bubbled into a sealed vial containing 30 mg (0.074 mmol) triphenylphosphonium dissolved in 500 μ L toluene at room temperature. After the ^{11}C radioactivity reached a plateau, the vial was heated to 140°C for 5 min, then solvents were removed in vacuo at 80°C. Absolute ethanol (5 mL) was added and the solution was again evaporated to dryness. With the vacuum removed, the radioligand was reconstituted with 7-mL sterile saline (0.9%) and passed through a 0.2- μ m sterile filter (Acrodisc; Gelman, New York, NY) into a sterile, pyrogen-free multidose vial. Sterile aqueous sodium bicarbonate (8.4%) was added to provide the final formulation (pH 7.4) for intravenous injection. All formulations were found to be sterile and pyrogen free by standard methods.

Synthesis of [^{68}Ga]EDTA

A $^{68}\text{Ge}/^{68}\text{Ga}$ generator (NEN, Boston, MA) was used. ^{68}Ga was eluted with 10 mL 1N HCl, filtered through a 0.22-mm Millipore filter into a 20-mL evacuated vial. Disodium ethylenediaminetetraacetic acid (EDTA) (0.15 mg dissolved in 0.1 mL saline) was added to the ionic ^{68}Ga solution and was mixed. The pH was adjusted to 7.4 with 12 mL 8.4% sterile sodium bicarbonate and the solution was filtered through a sterile 0.22- μ m Millipore filter.

PET Acquisition

A total of 10 PET scans were acquired in three dogs. Two of the three dogs underwent two sets of PET studies, 4 d before and 9 d after tumor inoculation. Each set involved paired coregistered PET studies: a [^{11}C]TPMP dynamic scan followed by a [^{68}Ga]EDTA dynamic scan. One dog underwent paired PET studies 9 d after tumor inoculation. Before the PET study, the dogs were anesthetized with intravenous sodium pentobarbital (35 mg/kg) and were intubated, and sterile catheters were placed in two leg veins for infusion of anesthetics and injection of the radiotracer and in the femoral artery for collection of blood. Systemic heparinization was used to prevent catheter thrombosis. The dogs were placed in a specially designed Plexiglas carrier-headholder, and the head was affixed with ear bars. Blood pressure, body temperature, oxygen saturation, end tidal CO_2 and heart rate were continuously monitored.

PET images were acquired on a GE 4096+ scanner (15 slices, 6.5-mm full width at half maximum; GE Medical Systems, Milwaukee, WI). The dogs were positioned in the scanner using the PET laser alignment line such that the cranial burr hole was centered in the PET field of view (slice 7). A 10-min transmission scan using a $^{68}\text{Ge}/^{68}\text{Ga}$ source was obtained for subsequent attenuation correction. After intravenous injection of 370 MBq (10 mCi) [^{11}C]TPMP, a series of 19 emission scans was acquired. The scan duration increased progressively from 30 s to 20 min for a total time of 115 min postinjection. Two hours after injection of [^{11}C]TPMP, 66.15 MBq (1.89 mCi) [^{68}Ga]EDTA were injected and emission scans were acquired under the same PET protocol. The dog's head was kept at the same position during the two PET studies allowing for subsequent coregistration of [^{11}C]TPMP and [^{68}Ga]EDTA images. PET scans were corrected for radioactivity

decay and for attenuation using the acquired transmission scans. Reconstruction was accomplished by 6-mm Hann filtered backprojection using a 26 \times 26-cm field of view projected onto a 128 \times 128 pixel matrix (2 \times 2-mm pixel size). Images were then smoothed using a 3 \times 3 pixel neighborhood averaging filter to a final resolution of 8.8 mm.

Arterial blood samples (0.5 mL) were collected through the femoral artery line at increasing time intervals from the start of the injection to the end of PET scanning. Blood samples were centrifuged (800g), plasma was separated and radioactivity concentration was determined in a gamma counter.

The second set of paired PET studies was performed under the same protocol. After the first set of paired PET studies, the dogs were transferred to the operating room, the catheters were removed under sterile conditions and skin incisions were closed. The dogs were placed in a warm blanketed cage in the recovery room and were monitored until complete recovery was achieved. After the second set of paired PET studies, the dogs were killed using an intravenous injection of 10 mL sodium pentobarbital.

Histology

The brains were removed from the cranium and were immersed in 10% neutral, buffered formalin solution. After a 1-wk fixation period, the brains were prepared for sectioning. Axial slices (3- to 5-mm thick) were cut parallel to the coronal imaging plane, for a distance well beyond the limits of the tumor boundaries. The tumors were easily seen on the cortical surface. The tissue blocks were embedded in paraffin and were cut in a stepwise fashion to obtain serial histological sections (7- μ m thick) at 1-mm increments. Histological sections ipsilateral and contralateral to the side of the tumor were taken. The sections were stained with hematoxylin and eosin. Histological sections were inspected by an experienced pathologist for evaluation of viable and necrotic tumor tissue and nontumor components such as edema and hemorrhage and regions of blood-brain barrier (BBB) defect.

Image and Data Analysis

In all three dogs, tumor tissue was confined to the injected brain hemisphere and was seen in two adjacent axial PET images. The slice containing the largest volume of tumor was selected for analysis. Temporal images of the selected slice, from 55 to 95 min, were summed to create an image for delineation of the regions of interest (ROIs). A rectangular ROI (4 \times 4 pixels) was drawn on the summed image in the tumor region of highest activity (tumor), and an ROI of similar size was drawn on the contralateral brain homologue (nontumor). The ROI's template was then placed on the temporal images covering 19 time frames of the corresponding slice to generate time-activity curves. The ROI's template was first drawn on the [^{11}C]TPMP image and was then transferred to the [^{68}Ga]EDTA image. [^{11}C]TPMP and [^{68}Ga]EDTA activity were corrected for decay. Tracer radioactivity is expressed in nCi/mL/mCi injected dose. Retention of [^{11}C]TPMP in the tumor region was evaluated by Patlak plot, entailing normalized brain activity versus normalized time: $\text{ROI}(t)/\text{Cp}(t)$ versus $\int_0^t \text{Cp}(t) dt/\text{Cp}(T)$ (27).

RESULTS

Histologically defined unilateral tumor growth was detected in the brain of all studied dogs. No histological evidence of tumor infiltration to the contralateral hemisphere was found. In the three studied dogs, tumor size in the long

axis was 1.4, 1.5 and 1.1 cm, respectively. The brain tissue harboring tumor was sedimented with uniformly distributed viable transformed cells, intertwined with sparse, small (0.01–0.03 mm) necrotic islands. In one dog, there was a large edematous region (Fig. 1C, arrow). Edema or hemorrhage was not seen in the other two dogs. Degradation of the BBB in the area of the tumor mass was identified histologically in all three dogs.

In all three dogs, [⁶⁸Ga]EDTA showed evidence of BBB defect at the site of the tumor and the activity of [¹¹C]TPMP at this site exceeded the activity in the normal brain. Increased uptake of [¹¹C]TPMP was more localized to the tumor area than to the area depicted by [⁶⁸Ga]EDTA. A qualitative visual comparison of PET images and histological sections revealed that the area of increased activity of [¹¹C]TPMP corresponded to the area of tumor infiltration. Figure 1 depicts an example of [¹¹C]TPMP and [⁶⁸Ga]EDTA images and a corresponding histological cross-section of the tumor. Increased uptake of [¹¹C]TPMP appears at the site of the tumor main mass, as well as in the region of tumor narrow infiltration propagating ventrally (Fig. 1, red arrow), but not in the adjacent edematous region (Fig. 1, green arrow). Conversely, [⁶⁸Ga]EDTA is uniformly distributed in an oval shape, which weakly correlates with the tumor boundaries (Fig. 1A).

[¹¹C]TPMP exhibited a rapid washout from blood. [¹¹C]TPMP activity in plasma peaked at 45–60 s and dropped sharply to very low values 1 min thereafter. [¹¹C]TPMP plasma activity over the 55- to 95-min time period was 1.4 ± 1.3 nCi/mL/mCi (mean \pm SD, $n = 5$). [⁶⁸Ga]EDTA exhibited slower kinetics than [¹¹C]TPMP. [⁶⁸Ga]EDTA plasma activity peaked at 45–60 s and gradually washed out reaching values of 34.2 ± 27.7 nCi/mL/mCi over the 55- to 95-min interval. [¹¹C]TPMP activity exhibited similar kinetics in the control brain (4 d before tumor inoculation) and in the brain contralateral to the tumor.

[¹¹C]TPMP activity in the intact brain was low, predominated by vascular activity (Fig. 2). [¹¹C]TPMP activity peaked to 38.1 ± 4.5 nCi/mL/mCi ($n = 5$) at 45–60 s and rapidly declined to 3.1 ± 1.5 nCi/mL/mCi 1 min thereafter, reaching a mean value of 1.8 ± 0.4 nCi/mL/mCi over the 55- to 95-min interval. [⁶⁸Ga]EDTA activity in the intact brain exhibited a gradual washout and activity over the 55- to 95-min interval was 8.2 ± 1.9 nCi/mL/mCi ($n = 5$) (Fig. 2).

In the tumor area, [¹¹C]TPMP peaked to values of 103 ± 8.7 nCi/mL/mCi ($n = 3$) at 45–60 s postinjection. Within a few minutes after the peak, [¹¹C]TPMP tumor activity declined to lower values that remained steady throughout the PET scan (Fig. 2). Unlike the steady concentration of [¹¹C]TPMP, [⁶⁸Ga]EDTA gradually washed out from tumor throughout the entire scanning period (Fig. 2). Patlak plot of [¹¹C]TPMP normalized activity in tumor, over the 20- to 95-min interval, is demonstrated in Figure 3. Patlak plot is linear over this interval with a high correlation coefficient ($r = 0.99$). Similar linear fit was observed in the other two dogs ($r = 0.97 \pm 0.01$). Table 1 summarizes [¹¹C]TPMP and [⁶⁸Ga]EDTA activity in tumor and contralateral brain. In the single dog with edema, [¹¹C]TPMP activity over the 55- to 95-min interval in the edematous region (2.1 nCi/mL/mCi) was similar to the activity measured in the contralateral brain (1.2 nCi/mL/mCi).

DISCUSSION

This investigation was initiated to determine whether the PET tracer [¹¹C]TPMP is suitable for imaging canine brain gliomas. The rationale for this investigation derived from in vitro and in vivo studies demonstrating a highly enhanced and selective accumulation of phosphonium cations in a variety of malignant cells, including human cerebral gliomas. In specimens taken from patients with brain tumors, [³H]TPP uptake in dispersed glioma cells was 40 times

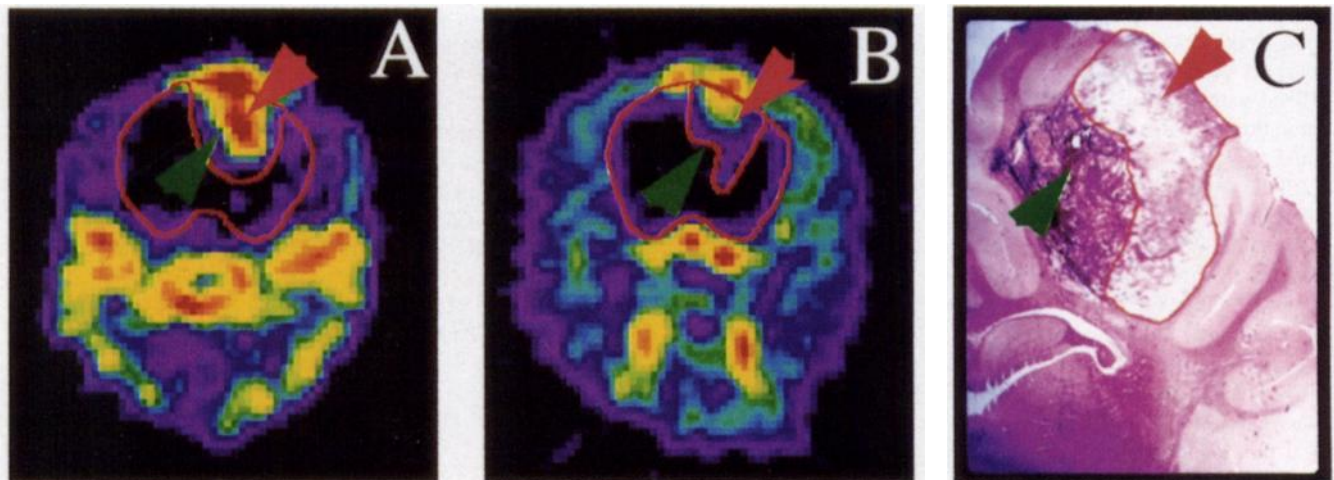


FIGURE 1. (A) Coregistered [¹¹C]TPMP and (B) [⁶⁸Ga]EDTA PET images and (C) corresponding histological section acquired 9 d after tumor inoculation. PET images represent averaged activity over 55- to 95-min postinjection interval. Each image is scaled to its own maximum value. Enhanced uptake of [¹¹C]TPMP overlaps tumor boundaries seen on histological section, including narrow ventral tumor infiltration (red arrow in B and C). Region of edema is seen next to tumor, and [¹¹C]TPMP uptake is not seen in edematous region (green arrow in B and C).

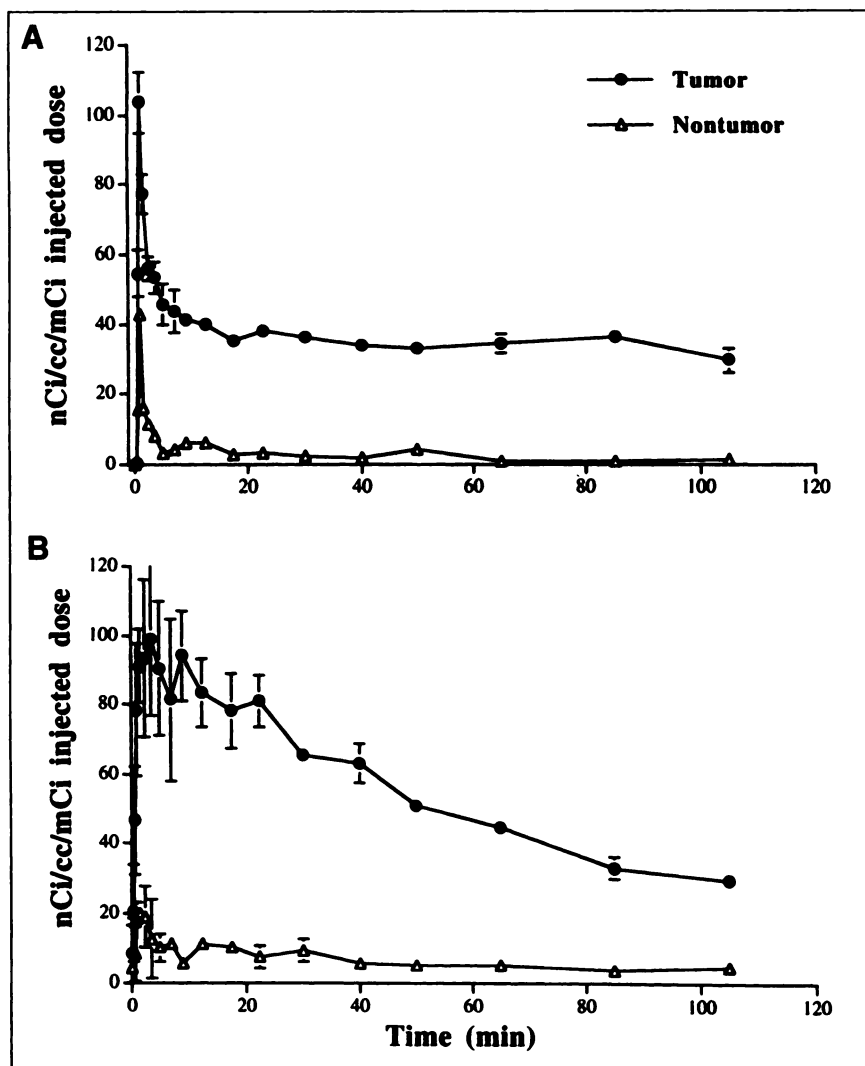


FIGURE 2. Time-activity curves of [¹¹C]TPMP (A) and [⁶⁸Ga]EDTA (B) in tumor region (Tumor) and in contralateral brain (Nontumor). Values represent mean of three dogs. Time points for brain radioactivity represent scan midtime. In tumor, [¹¹C]TPMP activity reaches plateau, whereas [⁶⁸Ga]EDTA exhibits gradual washout.

higher than in normal epithelial cells (15). In vitro studies have found a tight linear correlation between the transmembrane equilibrium distribution of phosphonium ions and the resting membrane potential measured by microelectrode recordings (18,20,28–32). Other studies provide evidence

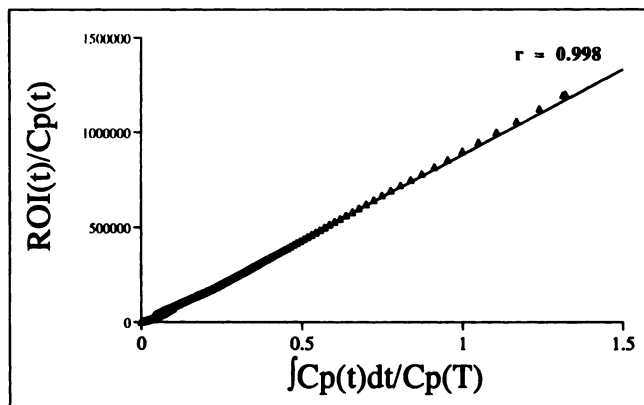


FIGURE 3. Patlak plot of data obtained during scanning from 0 to 95 min after injection of [¹¹C]TPMP. ROI = region of interest.

TABLE 1
[¹¹C]TPMP and [⁶⁸Ga]EDTA Accumulation in Canine Brain Glioma (Tumor) and Normal Brain (Nontumor) Tissue, over 55- to 95-Minute Interval, 9 Days After Tumor Cell Inoculation*

Dog	TPMP		
	Tumor	Nontumor	Tumor-to-nontumor ratio
1	38.3 ± 1.2	1.2 ± 0.6	31.9
2	33.3 ± 0.7	0.5 ± 0.4	66.6
3	35.2 ± 0.7	0.8 ± 0.2	44.0
Mean	35.6 ± 2.5	0.8 ± 0.4	47.5 ± 17.6
Dog	EDTA		
	Tumor	Nontumor	Tumor-to-nontumor ratio
1	38.5 ± 3.7	3.8 ± 1.5	10.1
2	40.3 ± 5.2	6.4 ± 0.2	6.3
3	42.5 ± 3.3	5.3 ± 0.7	8.0
Mean	40.4 ± 2.0	5.2 ± 1.3	8.1 ± 1.9

*Values expressed as nCi/mL/mCi injected dose (mean ± SD). TPMP = triphenylmethylphosphonium; EDTA = ethylenediamine-tetraacetic acid.

that the enhanced accumulation of phosphonium ions is correlated with increased negative potential differences across the plasma and mitochondria membranes of malignant cells (17,20). PET studies in beagle dogs have shown that depolarization of membrane potential by systemic administration of 40 mg/kg KCl resulted in an abrupt decrease of about 40%–50% in [¹¹C]TPMP concentration in heart muscle (26). In freshly prepared slices (0.5-mm thick) of the rat's hippocampus, depolarization of membrane potential by elevation of KCl concentrations in the incubation medium from 5 to 30 mmol/L caused a 30% decrease of [³H]TPP cellular accumulation (I. Madar and M. Segal, unpublished data, March 1998).

The major finding of this study is that under in vivo conditions, the PET tracer [¹¹C]TPMP is taken up by glioma cells rapidly and preferentially and is retained in the tumor area for a prolonged time resulting in a high tumor contrast. [¹¹C]TPMP exhibits a number of features that suggest its suitability for PET imaging of gliomas:

1. Rapid clearance from the blood. Mean [¹¹C]TPMP vascular activity, over a 2- to 10-min postinjection interval, is one fortieth of tumor activity. Although high-performance liquid chromatography studies for evaluation of metabolite fractions were not performed, the low blood radioactivity indicates that metabolites, if they exist, may contribute only a marginal fraction of the total activity.
2. Rapid and intense uptake in tumor. Under the present experimental conditions of blood withdrawal every 5–6 s and PET scanning every 15 s during the first 1 min postinjection, no discrepancy is found between time-to-peak activity in plasma and tumor, suggesting that [¹¹C]TPMP is a good perfusion agent with rapid extraction in tumor.
3. Prolonged retention in tumor tissue. As demonstrated in the graphical analysis, the Patlak plot is linear over the 20- to 95-min interval, indicating no loss of tracer from tumor cells over this time period. The steady [¹¹C]TPMP tumor concentration coincides with near zero values of [¹¹C]TPMP in plasma, suggesting that [¹¹C]TPMP is entrapped in tumor cells with minimal washout. The rapid extraction, marginal vascular activity and prolonged retention permit both quantification of [¹¹C]TPMP by relatively simple kinetic models and prolonged counting that provides better image statistics.
4. High tumor-to-nontumor ratio. [¹¹C]TPMP tumor uptake is 47.5 times higher than uptake in the contralateral hemisphere. This tumor contrast is one order of magnitude higher than the one reported in human glioma studies for other available PET and SPECT tracers (4,5,8,10,13).

A number of lipophilic cations for solid tumor imaging using PET and SPECT have been developed, including ⁸²Rb, ^{99m}Tc-sestamibi methoxyisobutyl isonitrile (MIBI) and ²⁰¹Tl

(4,5,13). Some contain a delocalized positive charge (e.g., MIBI). However, their tumor-to-nontumor uptake ratio is lower than that of [¹¹C]TPMP. Tumor-to-nontumor uptake ratio may range from 1.1 to 3.6 for MIBI (12) and from 1.2 to 2.4 for ²⁰¹Tl (9). ⁸²Rb has a lower tumor-to-nontumor uptake ratio and inconsistent retention (6). The differences in tumor contrast may result from different membrane transport mechanisms, such as potassium channels for Rb and sodium-potassium pump for ²⁰¹Tl, compared with the passive diffusion of [¹¹C]TPMP and from better coupling of tracer cellular accumulation with membrane potential, as demonstrated for [³H]TPP in comparison with ⁸²Rb (33). These factors may lead to a relatively more intense uptake of [¹¹C]TPMP in tumor cells and to a higher tumor-to-nontumor uptake ratio. Alternatively, species differences and differences in the tumor model may also contribute to the differences in the tracer's tumor selectivity. Results of this study indicate the highly preferential uptake of [¹¹C]TPMP in gliomas; however, further studies in humans are needed.

Animal studies have shown that the expected toxic effects of [¹¹C]TPMP may not prevent its use in humans. [³H]TPMP was shown to suppress tumor growth and colony formation, but to a lesser degree than ¹²³Rh and [³H]TPP (34). The estimated dose of [¹¹C]TPMP administered in humans (0.1 μg/kg; calculated according to a specific activity of 37,000 MBq [1,000 mCi] and a 740-MBq [20-mCi] injected dose) is far below the [³H]TPMP tolerated dose observed in mice (20 mg/kg) (34).

CONCLUSION

[¹¹C]TPMP exhibits a set of features essential for a good tracer for tumor delineation, including a rapid washout from blood, high uptake rate in tumor tissue, prolonged retention and a high tumor-to-nontumor uptake ratio. These features, along with the well-documented sensitivity of phosphonium ions to alterations in the transmembrane electrical gradient, may help develop a novel tool for membrane potential-based high-resolution tumor imaging as well as an investigative probe of tumorigenic processes through their manifestation in the cellular and mitochondrial membrane.

ACKNOWLEDGMENTS

The authors thank Michael A. Samphilipo, Jr., Carolyn A. Magee, and Paige A. Finley for their excellent technical assistance.

REFERENCES

1. Canellos GP. Residual mass in lymphoma may not be residual disease. *J Clin Oncol.* 1988;6:931–933.
2. Suit H, Lindberg R, Fletcher G. Prognosis significance of extent of tumor regression at completion of radiation therapy. *Radiology.* 1965;84:1100–1107.
3. Ancrì D, Basset JY, Lonchamps MF, Etavard C. Diagnosis of cerebral lesions by Thallium 201. *Radiology.* 1978;128:417–422.
4. Delbecke D, Meyerowitz C, Lapidus RL, et al. Optimal cutoff levels of F-18 fluorodeoxyglucose uptake in the differentiation of low-grade from high-grade brain tumors with PET. *Radiology.* 1995;195:47–52.

5. Doyle WK, Budinger TF, Valk PE, Levin VA, Gutin PH. Differentiation of cerebral radiation necrosis from tumor recurrence by [¹⁸F]FDG and ⁸²Rb positron emission tomography. *J Comput Assist Tomogr.* 1987;11:563-570.
6. Higashi K, Calvo AC, Whal RL. Does FDG uptake measure proliferative activity of human cancer cells? In vitro comparison with DNA flow cytometry and tritiated thymidine uptake. *J Nucl Med.* 1993;34:414-419.
7. Holzer T, Herholz K, Jeske J, Heiss WD. FDG-PET as a prognostic indicator in radiochemotherapy of glioblastoma. *J Comput Assist Tomogr.* 1993;17:681-687.
8. Herholz K, Holzer T, Bauer B, et al. ¹¹C-methionine PET for differential diagnosis of low-grade gliomas. *Neurology.* 1998;50:1316-1322.
9. Kim KT, Black KL, Marciano D. Thallium-201 SPECT imaging of brain tumors: methods and results. *J Nucl Med.* 1990;31:965-969.
10. Kubota K, Ishiwata K, Kubota R, et al. Tracer feasibility for monitoring tumor radiotherapy: a quadruple tracer study with fluorine-18-fluorodeoxyglucose or fluorine-18-fluorodeoxyuridine, L-[methyl-¹⁴C]methionine, [6-³H]thymidine, and gallium-67. *J Nucl Med.* 1991;32:2118-2123.
11. Ogawa T, Shishido F, Kanno I, et al. Cerebral glioma: evaluation with methionine PET. *Radiology.* 1993;186:45-53.
12. Park CH, Kim SM, Zhang J, McEwan JR, Intenzo C. Tc-99m MIBI brain SPECT of an acoustic schwannoma. *Clin Nucl Med.* 1994;19:152-154.
13. Vander-Borgh T, Pauwels S, Lambotte L, et al. Brain tumor imaging with PET and 2-[carbon-11]thymidine. *J Nucl Med.* 1994;35:974-982.
14. Davis S, Weiss MJ, Wong JR, Lampidis TJ, Chen LB. Mitochondrial and plasma membrane potentials cause unusual accumulation and retention of rhodamine 123 by human breast adenocarcinoma-derived MCF-7 cells. *J Biol Chem.* 1985;260:13844-13850.
15. Steichen JD, Weiss MJ, Elmaleh DR, Martuza RL. Enhanced *in vitro* uptake and retention of ³H-tetraphenylphosphonium by nervous system tumor cells. *J Neurosurg.* 1991;74:116-122.
16. Hiller R, Schaefer A, Zibirre R, Kaback HR, Koch G. Factors influencing the accumulation of tetraphenylphosphonium cation in HeLa cells. *Mol Cell Biol.* 1984;4:199-202.
17. Lampidis TJ, Hasin Y, Weiss MJ, Chen LB. Selective killing of carcinoma cells by lipophilic-cationic compounds: a cellular basis. *Biomed Pharmacother.* 1985;39:220-226.
18. Schuldiner S, Kaback HR. Membrane potential and active transport in membrane vesicles from *Escherichia coli*. *Biochemistry.* 1975;14:5451-5461.
19. Chen LB. Mitochondrial membrane potential in living cells. *Ann Rev Cell Biol.* 1988;4:155-181.
20. Lichtstein D, Dunlop K, Kaback HR, Blume AJ. Mechanism of monensin-induced hyperpolarization of neuroblastoma-glioma hybrid NG108-15. *Proc Natl Acad Sci USA.* 1979;76:2580-2584.
21. Beckman WC Jr, Powers SK, Brown JT, et al. Differential retention of rhodamine 123 by avian sarcoma virus-induced glioma and normal brain tissue of the rat *in vivo*. *Cancer.* 1987;59:266-270.
22. Powers SK, Ellington K. Selective retention of rhodamine-123 by malignant glioma in the rat. *J Neurooncol.* 1988;6:343-347.
23. Madar I, Weiss L, Chisin R. Enhanced uptake of [H-3]tetraphenylphosphonium (TPP) in malignant cell lines: *in vivo* studies in mice [abstract]. *J Nucl Med.* 1997;5:117P.
24. Wodinsky I, Kensler CJ, Roll DP. The induction and transplantation of brain tumors in neonatal beagles. *Proc Am Assoc Cancer Res.* 1969;10:99-103.
25. Anderson JH, Strandberg JD, Wong DF, et al. Multimodality correlative study of canine brain tumors. Proton magnetic resonance spectroscopy, positron emission tomography, and histology. *Invest Radiol.* 1994;29:597-605.
26. Fukuda H, Syrota A, Charbonneau P, et al. Use of ¹¹C-triphenylmethylphosphonium for the evaluation of membrane potential in the heart by positron emission tomography. *Eur J Nucl Med.* 1986;11:478-483.
27. Patlak CS, Blasberg RG, Fenstermacher JD. Graphical evaluation of blood-to-brain transfer constant from multiple-time uptake data. *J Cereb Blood Flow Metab.* 1983;3:1-7.
28. Demura M, Kamo N, Kobatake Y. Mitochondrial membrane potential estimated with the correction of probe binding. *Biochim Biophys Acta.* 1987;894:355-364.
29. Nakazato K, Murakami N, Konishi T, Hatano Y. Membrane potential in liposomes measured by the transmembrane distribution of ⁸⁶Rb⁺, tetraphenylphosphonium or triphenylmethylphosphonium: effect of cholesterol in the lipid bilayer. *Biochim Biophys Acta.* 1988;946:143-150.
30. Yorek MA, Dunlap JA. Resting membrane potential in 41A3 mouse neuroblastoma cells. Effect of increased glucose and galactose concentrations. *Biochim Biophys Acta.* 1991;1061:1-8.
31. Hockings PD, Rogers PJ. The measurement of transmembrane electrical potential with lipophilic cations. *Biochim Biophys Acta.* 1996;1282:101-106.
32. Mootha VK, French S, Balaban RS. Neutral carrier-based "Ca(2+)-selective" microelectrodes for the measurement of tetraphenylphosphonium. *Anal Biochem.* 1996;236:327-330.
33. Dorup I, Clausen T. ⁸⁶Rb is not a reliable tracer for potassium in skeletal muscle. *Biochem J.* 1994;302:745-751.
34. Pate J, Rideout D, McCarthy MR, et al. Antineoplastic activity, synergism, and antagonism of triarylalkylphosphonium salts and their combinations. *Anticancer Res.* 1994;14:21-28.